

# Next-to-leading order QCD corrections to the polarized hadroproduction of heavy flavors

Ingo Bojak

*Special Research Centre for the Subatomic Structure of Matter, Adelaide University, Adelaide SA 5005, Australia*

Marco Stratmann

*Institut für Theoretische Physik, Universität Regensburg, D-93040 Regensburg, Germany*

(Received 9 January 2002; revised manuscript received 22 November 2002; published 13 February 2003)

We present the complete next-to-leading order QCD corrections to the polarized hadroproduction of heavy flavors which soon will be studied experimentally in polarized  $pp$  collisions at the BNL Relativistic Heavy Ion Collider (RHIC) in order to constrain the polarized gluon density  $\Delta g$ . It is demonstrated that the dependence on unphysical renormalization and factorization scales is strongly reduced beyond the leading order. The sensitivity of the charm quark spin asymmetry to  $\Delta g$  is analyzed in some detail, including the limited detector acceptance for leptons from charm quark decays at the BNL RHIC.

DOI: 10.1103/PhysRevD.67.034010

PACS number(s): 12.38.Bx, 13.88.+e

## I. INTRODUCTION AND MOTIVATION

Triggered by the measurement of the proton's spin-dependent deep-inelastic structure function  $g_1^p$  by the European Muon Collaboration (EMC) [1] more than a decade ago, combined experimental and theoretical efforts have led to an improved understanding of the spin structure of the nucleon. In particular, we have gained some fairly precise information concerning the total quark spin contribution to the nucleon spin. The most prominent "unknown" is the elusive, yet unmeasured spin-dependent gluon density  $\Delta g$ . Hence current and future experiments, designed to further unravel the spin structure of the nucleon, focus strongly on the issue of constraining  $\Delta g$ . In particular, information will soon be gathered for the first time at the BNL Relativistic Heavy-Ion Collider (RHIC) [2].

The main thrust of the RHIC spin program [2] is to hunt down  $\Delta g$  by measuring double spin asymmetries in longitudinally polarized  $pp$  collisions at high energies. RHIC is particularly suited for this task, since the gluon density is expected to participate dominantly in many different production processes. This is in contrast with deep-inelastic lepton-nucleon scattering (DIS) where the gluon enters only as a small correction in the next-to-leading order (NLO) of QCD and indirectly via the renormalization group evolution of the parton densities. Along with the production of prompt photons and jets or hadrons with high transverse momentum  $p_T$ , heavy flavor pair creation is one of the most promising candidates at RHIC to study  $\Delta g(x, \mu_F)$  over a broad range of the momentum fraction  $x$  and scale  $\mu_F$ . For the first time, this allows us to verify the universality property of polarized parton densities, which is a consequence of the factorization theorem [3] and the foundation for the predictive power of perturbative QCD.

In the lowest order (LO) in the strong coupling  $\alpha_s$ , heavy flavor pair production in hadron-hadron collisions proceeds through two parton-parton subprocesses:

$$gg \rightarrow Q\bar{Q} \quad \text{and} \quad q\bar{q} \rightarrow Q\bar{Q}. \quad (1)$$

Gluon-gluon fusion is known to be the dominant mechanism

by far for charm and bottom quark production in the unpolarized case in all experimentally relevant regions of phase space [4–7]. This feature, true also in the polarized case unless  $\Delta g$  is exceedingly small, makes heavy quark production a particularly suited tool to study the gluon density. However, NLO QCD corrections to the LO subprocesses in Eq. (1) have to be included for a reliable description. First and foremost this is due to the strong dependence of the LO results on unphysical theoretical conventions such as the factorization scale, which reflects the amount of arbitrariness in the separation of short- and long-distance physics. In addition, the NLO corrections turn out to be quite sizable and not uniform in, e.g., the  $p_T$  of one of the heavy quarks [4,5]. The latter feature rules out the use of any approximations as estimates of the complete NLO corrections. The computation of the NLO corrections is fairly involved since one has to keep track of the mass of the heavy quark,  $m$ , throughout the calculation. Massless approximations are bound to fail at small-to-medium values of  $p_T$  where  $m \approx \mathcal{O}(p_T)$  and the cross section is large. So far only unpolarized NLO results have been available; see Refs. [4–6] and [7] for the differential and total cross sections, respectively. Polarized LO expressions can be found in Refs. [8,9], but the complete NLO results are presented for the first time in this work.

Apart from calculational difficulties, a further complication arises when one tries to match theoretical parton-level results for heavy flavor production rates with experimental ones. Experiments can only observe the remains of heavy quark (meson) decays—usually leptons. In practice they also have to impose a set of cuts on these particles to ensure a proper  $c$  and  $b$  quark separation and to take care of the usually limited and non-uniform detector acceptance. One thus has to find a practical way to incorporate hadronization, lepton-level cuts, and the detector acceptance in an analysis based on parton-level calculations, as they can distort spin asymmetries if polarized and unpolarized cross sections are affected differently. This may lead to incorrect conclusions about  $\Delta g$ . Heavy flavor decays usually have multi-body kinematics, making it difficult if not impossible to trace back cuts to the parton level analytically. Instead, for the time being, we propose to use “efficiencies,” to be defined below,

for bins in  $p_T$  and the pseudo-rapidity  $\eta$  of the heavy quark, to model its hadronization and decay as well as crucial detector features.

In this paper we focus mainly on the phenomenological applications of our results, in particular the production of heavy flavors at RHIC. Technical details and lengthy analytical results are omitted throughout and will be presented elsewhere [10]. In Sec. II we give, however, a brief survey of the main calculational steps and methods we have employed. In Sec. III we first discuss the different features of the NLO corrections to the total partonic subprocess cross sections, always in comparison to the unpolarized case. Next we demonstrate the significantly reduced dependence on unphysical renormalization and factorization scales in NLO QCD for heavy flavor production at RHIC. Finally, the sensitivity of the charm quark spin asymmetry at RHIC energies to  $\Delta g$  is studied in some detail, including realistic cuts on experimentally observable leptons from charm quark decays. We briefly outline further phenomenological applications of our results and conclude in Sec. IV.

## II. BRIEF OUTLINE OF THE TECHNICAL FRAMEWORK

The  $\mathcal{O}(\alpha_s^3)$  NLO QCD corrections to heavy flavor production are comprised of three parts: the one-loop virtual corrections to the LO processes in Eq. (1), the real “ $2 \rightarrow 3$ ” corrections with an additional gluon in the final state, and a new production mechanism,  $gq[\bar{q}] \rightarrow Q\bar{Q}q[\bar{q}]$ , appearing for the first time at the NLO level. We choose the well-established framework of  $n$ -dimensional regularization, with  $n=4+\epsilon$ , to tame the singularities of the loop and  $2 \rightarrow 3$  phase space integrals. Ultraviolet singularities show up only in the virtual corrections and are removed by on-shell mass and coupling constant renormalization at a scale  $\mu_R$ . The latter is performed in a variant of the modified minimal subtraction ( $\overline{\text{MS}}$ ) scheme which is usually adopted for heavy flavor production [6,7,5]. This prescription is characterized by the decoupling of heavy quark loop contributions to the gluon self-energy and leads to a fixed flavor scheme with  $n_{lf}=n_f-1$  light flavors active in the running of  $\alpha_s$  and in the scale  $\mu_F$  evolution of the parton densities. Infrared divergencies of the virtual diagrams are canceled by the real  $2 \rightarrow 3$  gluon bremsstrahlung corrections in the limit when the momentum of the final state gluon gets soft (“soft poles”). All remaining  $1/\epsilon$  singularities are associated with kinematical configurations when the momenta of two of the massless partons become collinear. They can be absorbed into the bare parton densities by the standard factorization procedure which we perform in the  $\overline{\text{MS}}$  scheme. The actual choice of the factorization scale  $\mu_F$  reflects the amount of arbitrariness in the separation of short-distance and long-distance physics and is therefore part of the theoretical uncertainties.

The required squared matrix elements  $|M|^2$  for both unpolarized and longitudinally polarized processes are obtained *simultaneously* by calculating them for arbitrary helicities  $\lambda_{1,2} = “\pm”$  of the incoming partons, i.e.,

$$|M|^2(\lambda_1, \lambda_2) = \overline{|M|^2} + \lambda_1 \lambda_2 \Delta |M|^2, \quad (2)$$

using the standard helicity projection operators for gluons and (anti-)quarks, i.e.,  $\epsilon_{\mu\nu\rho\sigma}$  and  $\gamma_5$  (see, e.g., Ref. [11]). Results obtained for the unpolarized part of Eq. (2),  $\overline{|M|^2}$ , can be compared to the literature [4–7], which serves as an important consistency check for the correctness of our new helicity dependent results  $\Delta |M|^2$ . To facilitate this comparison we closely follow the calculational steps and methods adopted in [4,5]. It should be noted that, contrary to the unpolarized case [5], the processes  $q\bar{q} \rightarrow Q\bar{Q}g$  and  $gq \rightarrow Q\bar{Q}q$  are *not* related by crossing for polarized initial states and have to be calculated from scratch. A subtlety arises in  $n$ -dimensionally regulated spin-dependent calculations beyond the LO of QCD. The Levi-Civita  $\epsilon$  tensor and  $\gamma_5$  are of purely four dimensional nature, and there exists no straightforward and unique generalization to  $n \neq 4$  dimensions. We treat them by applying the internally consistent ‘t Hooft–Veltman–Breitenlohner–Maison (HVBM) prescription [12]. The price to pay are  $(n-4)$  dimensional scalar products (“hat momenta”) appearing alongside the usual  $n$ -dimensional scalar products. In our case only a single hat momenta combination appears in the polarized  $2 \rightarrow 3$  cross section and can be accounted for by an appropriately modified phase space formula [13]. These contributions are inherently of  $\mathcal{O}(\epsilon)$  and only contribute to the final result when they pick up a  $1/\epsilon$  pole.

We should also recall here the definition of the spin-dependent parton densities and cross sections,

$$\Delta f(x, \mu_F) \equiv f_+^+(x, \mu_F) - f_-^+(x, \mu_F) \quad (3)$$

and

$$\Delta \sigma \equiv \frac{1}{2} [\sigma(+, +) - \sigma(+, -)], \quad (4)$$

respectively.  $f_+^+$  ( $f_-^+$ ) denotes the probability of finding a parton  $f=q, \bar{q}, g$  at a scale  $\mu_F$  with momentum fraction  $x$  and helicity  $+$  ( $-$ ) in a proton with helicity  $+$ . Similarly,  $\sigma(+, +)$  is the hadronic (partonic) cross section for the scattering of two hadrons (partons) with helicities  $+$ . The familiar unpolarized parton densities  $f(x, \mu_F)$  and cross sections  $\sigma$  are obtained by taking the sums in Eqs. (3) and (4), respectively. In the following, the compact notation  $\tilde{\phi}$  denotes *both* an unpolarized quantity  $\phi$  and its longitudinally polarized analogue  $\Delta \phi$ .

The virtual cross sections for the  $q\bar{q}$  and  $gg$  initial states are obtained up to  $\mathcal{O}(\alpha_s^3)$  from the interference between the virtual and Born amplitudes. Loop momenta in the numerator are dealt with by applying an adapted version of the Passarino-Veltman reduction program to scalar integrals [14], which properly accounts for all possible  $n$ -dimensionally regulated divergencies in QCD. The required scalar integrals can be found in [4]; however, we have checked them by standard Feynman parametrization techniques (see also [15]). Phase space integrations for the real  $2 \rightarrow 3$  gluon bremsstrahlung corrections for the  $q\bar{q}$  and  $gg$  initial states and the genuine NLO  $gq$  subprocess are subtle and require some care. As in [4,5] we are interested here in

the double differential single inclusive cross section for the production of a heavy quark (or antiquark). For stable numerical simulations it is advantageous to perform the integrations over the phase space of the two not observed partons *analytically* as far as possible. To achieve this requires extensive partial fractioning to reduce all phase space integrals to a standard form [4,13,15]. A sufficient set of four- and  $n$ -dimensional integrals are again conveniently collected in [4], but we have recalculated and confirmed this set.

The final color-averaged results for the dominant  $gg$  fusion process (and similarly for the other subprocesses) can be decomposed according to their color structure as

$$|\tilde{M}_{gg}|^2 = g^6 \tilde{E}_e^2 \frac{1}{2(N_C^2 - 1)} [(2C_F)^2 \tilde{M}_{\text{QED}} + C_A^2 \tilde{M}_{\text{OQ}} + \tilde{M}_{\text{KQ}} + 2C_F \tilde{M}_{\text{RF}} + C_A \tilde{M}_{\text{QL}}], \quad (5)$$

where  $g^2 = 4\pi\alpha_s$ ,  $E_e = 1/(1 + \varepsilon/2)$ , and  $\Delta E_e = 1$ . All color factors are expressed in terms of the Casimir operators  $C_F = (N_C^2 - 1)/2N_C$  and  $C_A = N_C$ , where  $N_C$  denotes the number of colors. We will analyze the different contributions to the total partonic  $gg$  cross section, Eq. (5), in Sec. III. Such a color decomposition is also of importance for converting our results for heavy quarks to the spin-dependent production of gluino pairs which we will discuss briefly in Sec. IV. It should be noted that we have imposed a slightly different way of splitting up the results according to color in Eq. (5) than in Ref. [4]. The choice in Eq. (5) ensures that the “Abelian”  $\tilde{M}_{\text{QED}}$  is identical to the QED part of  $\gamma g \rightarrow Q\bar{Q}$  in Ref. [13] after taking into account the usual factor  $1/(2N_C)$  for replacing a photon by a gluon. Furthermore, compared to Ref. [4] an additional function  $\tilde{M}_{\text{RF}}$  appears in Eq. (5) since we are interested in the general case  $\mu_R \neq \mu_F$ . For the soft-gluon plus virtual (S+V) part of Eq. (5) our unpolarized results fully agree analytically with the corresponding expressions in [4,5] except for  $M_{\text{QL}}$  in Eq. (6.22) of Ref. [4] which contains a numerically irrelevant misprint.<sup>1</sup> In the spin-dependent, case analytical results for the S+V cross sections will be given in [10]. As in the unpolarized case [4,5], the expressions for the gluon bremsstrahlung part of Eq. (5) are too lengthy to be published analytically but can be found in our computer code which will be made available upon request.

### III. NUMERICAL RESULTS AND PHENOMENOLOGICAL ASPECTS

Before presenting results for hadronic heavy flavor distributions we first discuss the *total partonic* subprocess cross sections  $\tilde{\sigma}_{ij}$ ,  $i, j = q, \bar{q}, g$ . They can be expressed in terms of LO and NLO functions  $\tilde{f}_{ij}^{(0)}$  and  $\tilde{f}_{ij}^{(1)}$ ,  $\tilde{f}_{ij}^{(1)}$ , respectively, which depend only on a single *scaling* variable  $\xi = s/(4m^2) - 1$ :

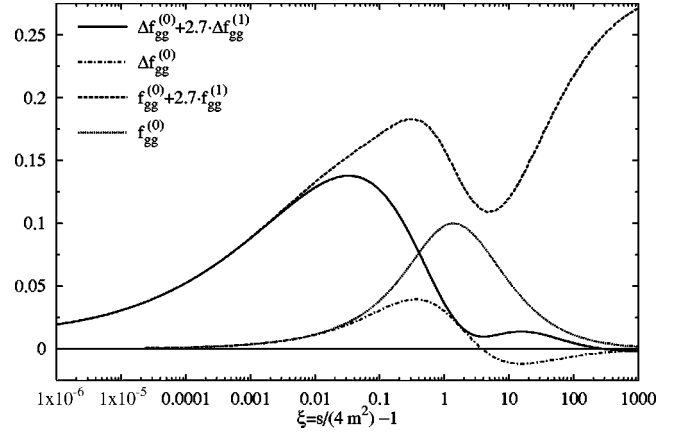


FIG. 1.  $(m^2/\alpha_s^2)\tilde{\sigma}_{gg}$  in NLO ( $\overline{\text{MS}}$ ) and LO as a function of  $\xi$  according to Eq. (6), where we have set  $\mu_F = \mu_R = m$  for simplicity and  $4\pi\alpha_s = 2.7$  as appropriate for charm production.

$$\tilde{\sigma}_{ij}(s, m^2, \mu_F, \mu_R) = \frac{\alpha_s^2}{m^2} \left\{ \tilde{f}_{ij}^{(0)}(\xi) + 4\pi\alpha_s \left[ \tilde{f}_{ij}^{(1)}(\xi) + \tilde{f}_{ij}^{(1)}(\xi) \ln \frac{\mu_F^2}{m^2} + \frac{\beta_0}{8\pi^2} \tilde{f}_{ij}^{(0)}(\xi) \ln \frac{\mu_R^2}{\mu_F^2} \right] \right\}, \quad (6)$$

where  $s$  is the available partonic center of mass system (c.m.s.) energy squared,  $\alpha_s = \alpha_s(\mu_R^2)$ , and  $\beta_0 = (11C_A - 2n_f)/3$ . Hence the  $\tilde{\sigma}_{ij}$  are particularly suited for studying the main features of the NLO corrections in the most transparent way. The  $\tilde{f}_{ij}^{(1)}$  are non-trivial functions of  $\xi$  and can be easily obtained from our double differential analytical results for the partonic cross sections by numerical integrations. In the unpolarized case they have been cast into a compact semi-analytical form [7] for fast numerical calculations of the total hadronic heavy flavor cross section which is a desirable future project also in the polarized case. The  $\tilde{f}_{ij}^{(1)}$  can be derived just from mass factorization, the only source for terms proportional to  $\ln \mu_F^2/m^2$ . The last term in Eq. (6) vanishes for the standard choice  $\mu_F = \mu_R$ . In NLO this term follows straightforwardly from the LO result by replacing  $\alpha_s(\mu_F^2) \rightarrow \alpha_s(\mu_R^2)[1 + \alpha_s(\mu_R^2)(\beta_0/4\pi) \ln(\mu_R^2/\mu_F^2)]$  thanks to the renormalization group invariance of the cross section.

In Fig. 1 we present the gluon-gluon subprocess cross section  $(m^2/\alpha_s^2)\tilde{\sigma}_{gg}$  in LO and NLO for  $\mu_F = \mu_R = m$  as a function of  $\xi$  in the  $\overline{\text{MS}}$  scheme. The threshold for  $Q\bar{Q}$  production,  $s = 4m^2$ , is located at  $\xi = 0$ . It turns out that the NLO corrections are significant in the entire  $\xi$  range. At threshold the polarized and unpolarized cross sections are equal; thus Eq. (2) implies that  $|M_{gg}|^2(+ -) \rightarrow 0$  as  $\xi \rightarrow 0$ . Unlike in LO where  $\tilde{\sigma}_{gg}$  approaches zero at threshold, it tends to a constant in NLO,  $(\alpha_s^3/8m^2)[1/2(N_C^2 - 1)] \times [(2C_F)^2 - C_A^2 + 5/2]\pi^2$ , due to the “Coulomb singularity” present in the S+V part. It should be noted that in the threshold region logarithms from soft gluon emissions also contrib-

<sup>1</sup>We thank J. Smith for his help in clarifying this issue.



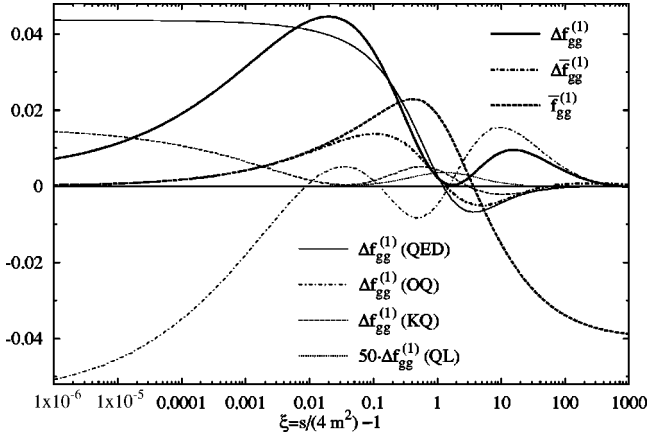


FIG. 2. Breakdown of the NLO ( $\overline{\text{MS}}$ ) coefficient function  $\Delta f_{gg}^{(1)}$  into contributions from different color factors according to Eq. (5). The numerically tiny quark-loop (QL) contribution is enhanced by a factor of 50. Also shown are the NLO coefficient functions  $\Delta \tilde{f}_{gg}^{(1)}$  and  $\tilde{f}_{gg}^{(1)}$  in Eq. (6) which arise from mass factorization.

ute significantly even down to the smallest  $\xi$  shown. In the high energy domain,  $\xi \rightarrow \infty$ , our polarized and unpolarized results behave rather differently. Here Feynman diagrams with a gluon exchange in the  $t$  channel drive the unpolarized NLO result to a plateau value [4] whereas the polarized NLO cross section vanishes like the LO one, i.e.,  $|M_{gg}|^2(++) \rightarrow |M_{gg}|^2(+-)$  in Eq. (2) as  $\xi \rightarrow \infty$ . Similar observations have been made in the photoproduction case  $\gamma g \rightarrow Q\bar{Q}$  [13]. It is important to point out that all the large deviations between NLO and LO arise from Feynman diagram topologies that occur for the first time at the NLO level. Beyond NLO no fundamentally new topologies are introduced and hence NLO results can be considered in a way as the first “complete” order. Considerable efforts have been made to push unpolarized calculations beyond the NLO of QCD by including resummations of large logarithms which appear to all orders in  $\alpha_s$  in the cross section. For instance, resummations of threshold logarithms have reached next-to-next-to-leading order accuracy [16]. They are of some importance if the cross section receives large contributions from or near the partonic threshold,  $s = 4m^2$ , as for  $t\bar{t}$  production at the Fermilab Tevatron or  $b\bar{b}$  rates at fixed target energies. Phenomenological studies of the impact of resummations on polarized heavy flavor cross sections are not yet available.

Figure 2 shows the decomposition of the polarized NLO ( $\overline{\text{MS}}$ ) coefficient function  $\Delta f_{gg}^{(1)}$  into contributions with different color structures as defined in Eq. (5). Notable are the large cancellations between the QED and the OQ contributions in the threshold region  $\xi \rightarrow 0$ . For completeness we also present here the coefficient functions  $\Delta \tilde{f}_{gg}^{(1)}$  and  $\tilde{f}_{gg}^{(1)}$  in Eq. (6) which arise from the mass factorization procedure. They exhibit a similar behavior for asymptotically small and large  $\xi$  as the NLO coefficient functions  $\Delta f_{gg}^{(1)}$  and  $f_{gg}^{(1)}$ . The scaling function  $\tilde{f}_{q\bar{q}}$  satisfies the expected relation  $\Delta f_{q\bar{q}} = -f_{q\bar{q}}$ , but only after taking into account an additional finite factorization to undo the unphysical helicity violation at the  $q\bar{q}g$  vertex in the HVBM scheme, which is reflected by the

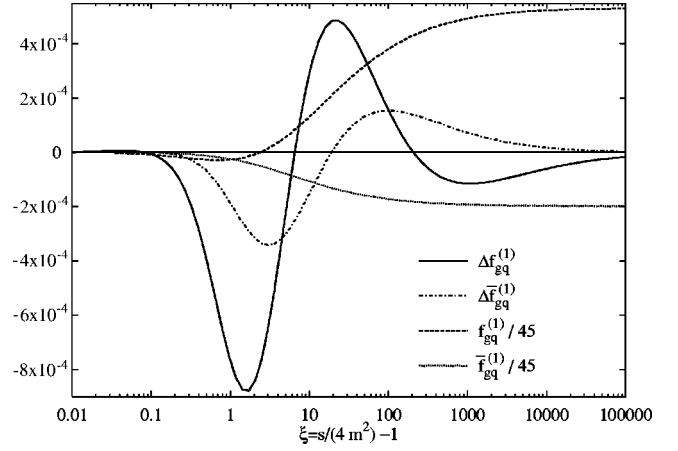


FIG. 3. The genuine NLO ( $\overline{\text{MS}}$ ) coefficient functions  $\tilde{f}_{gq}^{(1)}$  and  $\tilde{f}_{gq}^{(1)}$  as a function of  $\xi$ .

mismatch of the polarized and unpolarized LO  $q\bar{q}$  splitting functions in  $n$  dimensions [17], i.e.,  $P_{q\bar{q}}^{(0)} \neq \Delta P_{q\bar{q}}^{(0)}$ . The behavior of  $f_{q\bar{q}}$  was already discussed in [5] and will not be repeated here. The genuine NLO scaling functions  $\tilde{f}_{gq}$  are numerically much smaller than  $\tilde{f}_{gg}$  as can be inferred from comparing Figs. 1 and 3. The  $\tilde{f}_{gq}$  exhibit the same high-energy  $\xi \rightarrow \infty$  behavior as  $\tilde{f}_{gg}$ , i.e.,  $f_{gq}$  approaches a plateau while  $\Delta f_{gq}$  vanishes.

The physical, i.e., experimentally observable, total cross section is obtained by convoluting the partonic cross sections in Eq. (6) with the appropriate combinations of parton densities evolved to the scale  $\mu_F$ ,

$$\tilde{\sigma}(S, m^2, \mu_F, \mu_R) = \sum_{ij} \int_{x_{\min}}^1 dx_1 \int_{x_{\min}/x_1}^1 dx_2 \tilde{f}_i(x_1, \mu_F) \times \tilde{f}_j(x_2, \mu_F) \tilde{\sigma}_{ij}(s, m^2, \mu_F, \mu_R), \quad (7)$$

where  $S$  is the available hadron-hadron c.m.s. energy squared,  $s = x_1 x_2 S$ , and  $x_{\min} = 4m^2/S$ . In a similar fashion, differential heavy (anti-)quark inclusive distributions, like  $d^2\tilde{\sigma}/dp_T d\eta$ , can be derived by convolution with appropriate double differential partonic cross sections. It also should be kept in mind that beyond the LO of QCD, parton densities and partonic cross sections have to be taken in the same factorization scheme in order to guarantee that Eq. (7) is independent of unphysical theoretical conventions up to the order in  $\alpha_s$  considered in the calculation.

One of the main motivations for performing the NLO calculations was to reduce the dependence on the actual choice of  $\mu_F$  and  $\mu_R$  which is completely arbitrary in LO and can lead to sizable ambiguities in predictions for  $\tilde{\sigma}(S, m^2)$  and the corresponding spin asymmetry to be defined below. In Fig. 4 we demonstrate that the NLO results for the polarized charm production cross section are indeed more robust under scale variations than LO estimates. In the left panel of Fig. 4 we vary  $\mu_F$  and  $\mu_R$  independently of each other in the range  $\mu_R^2 = Rm^2$  and  $\mu_F^2 = Fm^2$  with  $1 \leq (R, F) \leq 4.5$  for fixed  $m = 1.4$  GeV at a typical RHIC energy of  $\sqrt{S} = 200$  GeV using

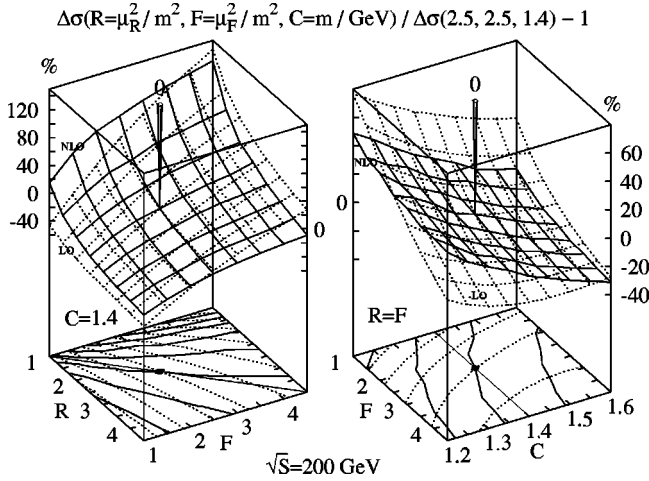


FIG. 4. Deviation (in %) of the polarized total charm cross section in LO (dotted) and NLO (solid) from a reference choice (“0-pin” marker, see text): left part, as a function of  $\mu_F$  and  $\mu_R$  for fixed  $m$ ; right part, as a function of  $\mu_F$  and  $m$  with  $\mu_R = \mu_F$  (here the LO result is multiplied by a factor of  $-1$ ). Corresponding contour lines in steps of 20% are given at the base of each plot.

the Glück-Reya-Stratmann-Vogelsang (GRSV) “standard” set of polarized parton densities [18]. In the right part of Fig. 4 we employ the conventional choice  $\mu_R = \mu_F$  and vary  $\mu_F$  and  $m = C$  GeV in a typical range for the charm quark pole mass,  $1.2 \leq C \leq 1.6$ . In order to better visualize the uncertainties due to scale and mass variations we show  $\Delta\sigma(R, F, C)/\Delta\sigma(R=2.5, F=2.5, C=1.4) - 1$ , i.e., the deviation in percent of the total polarized charm production cross section according to Eq. (7) for variable  $\mu_{F,R}$  and  $m$  with respect to a reference cross section taken at fixed  $\mu_F^2 = \mu_R^2 = 2.5m^2$  with  $m = 1.4$  GeV. To better guide the eye, contour lines in steps of 20% are plotted at the base of each plot. Here we also indicate the common choice  $\mu_R = \mu_F$  and  $m = 1.4$  GeV (thin solid lines) in the left and right part, respectively.

The NLO result in the left part of Fig. 4 is considerably “flatter” than the LO result with respect to variations of  $\mu_F$  but shows, however, slightly more variation with  $\mu_R$ . Not unexpectedly and more importantly it turns out that the usual choice  $\mu_R = \mu_F$  almost coincides with the contour line of zero deviation from the reference cross section in NLO, in stark contrast to the situation at LO. This leads to the improved stability of the NLO prediction as observed in the right panel of Fig. 4 for variations of a common scale  $\mu_R = \mu_F$  at a given charm quark mass  $m$ . Here variations of the charm mass cause the major uncertainty of about  $\pm 30\%$  in the NLO predictions. In LO we find considerable uncertainty stemming from variations of  $\mu_F$  on top of that. It should also be noted that qualitatively similar results are obtained for  $\sqrt{S} = 500$  GeV and bottom quark production at RHIC. Usually, in the NLO terms proportional to  $\ln \mu_F^2/m^2$  and  $\ln \mu_R^2/\mu_F^2$  in Eq. (6) start to have a compensating effect for different choices of  $\mu_F$  and  $\mu_R$  and also provide some guidance that  $\mu_F \sim \mathcal{O}(m)$  and  $\mu_F \sim \mu_R$  in order to avoid large logarithms in the hard partonic cross sections. Ultimately, one expects the dependence on  $\mu_F$  and  $\mu_R$  to be reduced more and more if

higher and higher orders in  $\alpha_s$  are considered. However, as was briefly explained above in connection with Fig. 1, in the reaction studied here new types of Feynman diagram topologies enter the calculation for the first time at the NLO level, whereas in next-to-NLO (NNLO) and beyond no qualitatively different diagrams appear. Hence in a sense NLO is the first “complete,” non-trivial order of perturbation theory for heavy flavor production, and it is pleasing that scale stability improvements nevertheless clearly set in without considering NNLO corrections which seem unattainable in the foreseeable future.

Instead of measuring polarized cross sections like  $\Delta\sigma(S, m^2)$  directly, experiments will usually study the related longitudinal spin asymmetry defined by

$$A(S, m^2) \equiv \frac{\Delta\sigma(S, m^2)}{\sigma(S, m^2)} \quad (8)$$

in case of the total cross section and accordingly for differential heavy quark distributions. The experimental advantage of this quantity is that one does not need to determine the absolute normalization of the cross sections  $\tilde{\sigma}(S, m^2)$  which is usually difficult to obtain. However, one should keep in mind that the situation in the unpolarized case is far from clear, in particular concerning bottom quark production [19], and hence it would be reasonable and helpful to determine the unpolarized and polarized cross sections separately. We note that for small variations of the scales the relative deviation of the asymmetry can be written as  $\delta A/A = \delta\Delta\sigma/\Delta\sigma - \delta\sigma/\sigma$ . It turns out for the variations of  $\mu_F$ ,  $\mu_R$ , and  $m$  considered above that  $\delta\Delta\sigma/\Delta\sigma$  and  $\delta\sigma/\sigma$  are almost equal in NLO, whereas they can differ strongly in LO. As a result it is even more true for the asymmetry that NLO results are highly stable, whereas the LO uncertainty is huge, in particular for the choice  $\mu_R = \mu_F$ . We will explore this in detail in [10], but wish to point out here that LO determinations of  $\Delta g$  using the asymmetry alone will necessarily have a prohibitively large theoretical error, so that a NLO analysis is a must in that case.

Finally, let us turn to the important question of whether heavy flavor production at RHIC can be used to discriminate between different polarized gluon densities. To address this question thoroughly one has to take into account an estimate of the statistical significance of a measurement of a heavy quark spin asymmetry at RHIC. Compared to direct photons or jets, which are directly observed in the detector, this is a rather involved problem for heavy flavors. With the PHENIX detector at RHIC charm and bottom quarks can be identified only through their decay products, preferably leptons. However, the electron and muon detection is rather limited in pseudo-rapidity,  $|\eta_e| \leq 0.35$  and  $1.2 \leq |\eta_\mu| \leq 2.4$ , respectively, and cuts in the lepton  $p_T$  have to be imposed in order to separate charm and bottom quarks. Since heavy flavor decays usually have a multi-body kinematics and may proceed through “cascades,” cuts on the observed leptons are difficult to translate back to the calculated parton, i.e., heavy quark, level. One possibility is to rely on Monte Carlo simulations of heavy quark decays, for instance, on PYTHIA [20],

which are quite successful and tuned to a wealth of data. PYTHIA can be used to generate “efficiencies”  $\varepsilon_{\text{eff}}$  for observing a heavy quark within a certain bin in  $p_T$  and  $\eta$  in the detectors at RHIC. Ideally, if properly normalized to the total number of heavy quarks generated in that particular bin,  $\varepsilon_{\text{eff}}$  should become independent of all the details of the heavy quark production mechanism assumed in PYTHIA. However, the string fragmentation used in PYTHIA inseparably links the hadronization to the production environment which is modeled by LO matrix elements accompanied by parton showers [20,21]. Luckily, the efficiencies for the single electron tag,  $c, b \rightarrow eX$  with  $|\eta_e| \leq 0.35$ , used at PHENIX and studied in the following, are rather insensitive to having initial and/or final state parton showers switched on or off in PYTHIA. In addition, the so-called “color drag effect” is inherently a low  $p_T$  and high  $\eta$  phenomenon [21] and hence should be also of minor importance for the single electron tag,  $c, b \rightarrow eX$ .

Exploiting this idea, a first numerical study for the PHENIX detector has been performed. The resulting efficiency  $\varepsilon_{\text{eff}}(p_T, \eta)$  for a charm quark produced with transverse momentum  $p_T$  and pseudo-rapidity  $\eta$  to be detected via its decay electron *anywhere* in the PHENIX acceptance, with the electron trigger allowing  $p_T^e > 1$  GeV, is approximately given by

$$\varepsilon_{\text{eff}}(p_T, \eta; p_T^e > 1 \text{ GeV}) = \zeta \exp\left(\frac{-9.79 + 4.58(p_T/\text{GeV})^{1.88}}{(p_T/\text{GeV})^{1.73} + 1.74\zeta^{-0.79}}\right) \quad (9)$$

with

$$\zeta = \exp\{-|\eta|/4.06\} \times \exp[-(p_T/1.05 \text{ GeV})^{0.43}] [5.84 \exp[-(p_T/2.48 \text{ GeV})^{0.42}]]$$

A prediction for the charm cross section as measurable with PHENIX is then obtained by convoluting our double differential partonic results with  $\varepsilon_{\text{eff}}$  in Eq. (9),

$$\tilde{\sigma}_{\text{eff}}(p_T^e > 1 \text{ GeV}) = \int_0^{p_T^{\text{max}}} dp_T \int_{-\eta^{\text{max}}}^{\eta^{\text{max}}} d\eta \varepsilon_{\text{eff}}(p_T, \eta; p_T^e > 1 \text{ GeV}) \frac{d^2 \tilde{\sigma}}{dp_T d\eta}, \quad (10)$$

where  $p_T^{\text{max}} = \frac{1}{2} \sqrt{S - 4m^2}$  and  $\eta^{\text{max}} = -\frac{1}{2} \ln[1 - \sqrt{1 - 4p_T^2/(S - 4m^2)}]/[1 + \sqrt{1 - 4p_T^2/(S - 4m^2)}]$  are the appropriate kinematical limits. Different cuts in  $p_T^e$  are simulated by limiting the charm transverse momentum  $p_T$  instead, while still using Eq. (9), i.e.,

<sup>2</sup>We are grateful to M. Grosse Perdekamp from PHENIX for providing these efficiencies.

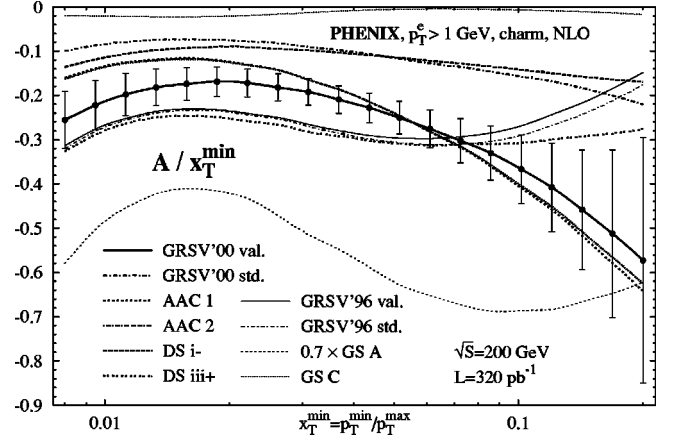


FIG. 5. The NLO charm asymmetry  $A$  at  $\sqrt{S}=200\text{GeV}$  for PHENIX at RHIC as a function of  $x_T^{\text{min}}=p_T^{\text{min}}/p_T^{\text{max}}$  using Eq. (11). For a better separation of the curves  $A$  is rescaled by  $1/x_T^{\text{min}}$ . Recent and old sets of helicity densities are distinguished by thick and thin lines, respectively. Also shown is an estimate for the statistical error using a luminosity of  $\mathcal{L}=320\text{pb}^{-1}$  (see text).

$$\tilde{\sigma}_{\text{eff}}(p_T^e > p_T^{\text{min}}) \approx \int_{p_T^{\text{min}}}^{p_T^{\text{max}}} dp_T \int_{-\eta^{\text{max}}}^{\eta^{\text{max}}} d\eta \times \varepsilon_{\text{eff}}(p_T, \eta; p_T^e > 1 \text{ GeV}) \frac{d^2 \tilde{\sigma}}{dp_T d\eta}. \quad (11)$$

This expression has been used for the results shown in Figs. 5, 6, and 7 below. Of course, more detailed and improved studies have to accompany future extractions of  $\Delta g$  at RHIC, in particular for channels other than  $c, b \rightarrow eX$ . Ultimately, efficiencies based on NLO matrix elements rather than the LO ones used in PYTHIA are desirable if not necessary.

To study the sensitivity of the charm production asymmetry at RHIC to  $\Delta g$  in Fig. 5, we use a wide range of different sets of helicity densities [18,22,23], including also

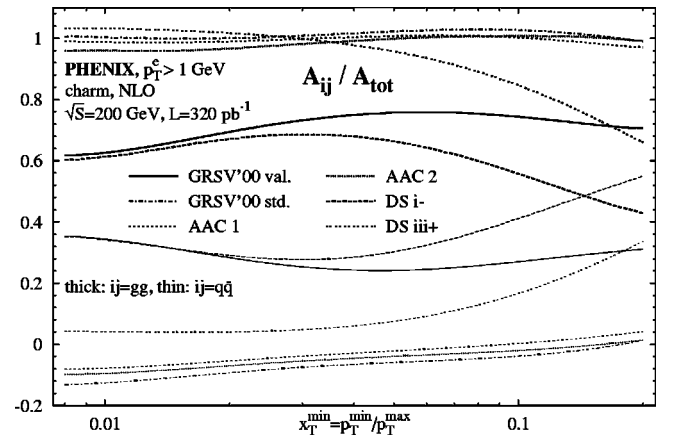


FIG. 6. Contributions to the NLO charm spin asymmetry of Fig. 5 from  $gg$  and  $q\bar{q}$  subprocesses according to Eq. (12) for several sets of polarized parton densities [18,22,23].



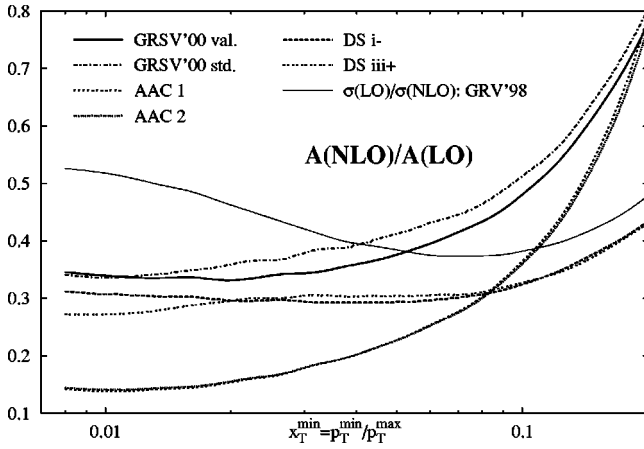


FIG. 7. Ratio of the asymmetries in NLO and LO,  $A(\text{NLO})/A(\text{LO})$ , with  $A(\text{NLO})$  as shown in Fig. 5. The ratio of unpolarized cross sections  $\sigma(\text{LO})/\sigma(\text{NLO})$  used in the calculation of  $A$  is also shown for comparison (thin solid line).

some of the older analyses [24,25], which, nevertheless, still give a rather good description of all available DIS data. All sets mainly differ in the assumptions about  $\Delta g$ . Note that for calculating the required unpolarized  $\sigma$  in  $A = \Delta\sigma/\sigma$  we have used in each case the underlying set of helicity averaged parton distributions as specified in [18,22–25] as well as the value for  $m$  assumed in these fits ( $m = 1.4$  or  $1.5$  GeV). All results are obtained for the choice  $\mu_F^2 = \mu_R^2 = 2.5(m^2 + p_T^2)$ . It is immediately apparent from Fig. 5 that charm production at RHIC can be very useful in pinning down  $\Delta g$ . The estimated statistical error for such a measurement,  $\delta A = \{1/P_p^2\} \{1/\sqrt{\mathcal{L}\sigma_{\text{eff}}}\}$ , assuming a luminosity of  $\mathcal{L} = 320 \text{ pb}^{-1}$  and a beam polarization of  $P_p \approx 0.7$  [2], is significantly smaller than the total spread of the predictions. The asymmetry obtained for the large  $\Delta g$  of Gehrman-Stirling set A (GS A) [25] had to be scaled down by 0.7 to fit well into the same plot. Not unexpectedly, very small gluons, e.g., the oscillating  $\Delta g$  of GS C [25], yield an almost vanishing asymmetry in the entire range of  $x_T^{\text{min}}$  shown in Fig. 5. We note that in each bin  $\Delta g$  is predominantly probed at  $x$  values around  $x_1 \approx x_2 \approx x_T^{\text{min}}$ . We will map the range in  $x$  where  $\Delta g$  is accessible by heavy flavor production at RHIC in more detail in [10].

To investigate the sensitivity of charm production to  $\Delta g$  at RHIC even further, we split up the spin asymmetry shown in Fig. 5 into contributions from different subprocesses by defining

$$\frac{A_{ij}}{A_{\text{tot}}} = \frac{\Delta\sigma_{ij}}{\Delta\sigma_{\text{tot}}}, \quad (12)$$

where  $ij = \{gg, gq, q\bar{q}\}$ .  $A_{\text{tot}}$  and  $\Delta\sigma_{\text{tot}}$  denote the total spin asymmetry and cross section, respectively. Figure 6 shows the contribution of the gluon-gluon fusion and quark-antiquark annihilation subprocesses to the total charm spin asymmetry as shown in Fig. 5 for several sets of parton densities [18,22,23]. The contribution of the  $gq$  induced subprocess can be easily deduced from  $A_{\text{tot}} = A_{gg} + A_{q\bar{q}} + A_{gq}$ .

As expected, the major contribution to the spin asymmetry stems from  $A_{gg}$ . Even for rather small gluon densities like the de Florian–Sassot set i– (DS i–) still about 60% of  $A$  come from gluon-gluon fusion. In addition, one observes for all sets of parton densities cancellations between  $q\bar{q}$  and  $gq$  induced subprocesses, further enhancing the dominance of the  $gg$  channel. Only for the very small and oscillating  $\Delta g$  of GS C [25] is the tiny spin asymmetry (see Fig. 5) mainly due to quark-antiquark annihilation. In conclusion, there is a clear correlation between the size of  $\Delta g$  and the observed spin asymmetry. We have also verified that this result is not spoiled by the rather strong dependence of the polarized and unpolarized cross sections on the heavy quark mass discussed above (see Fig. 4). It turns out that the spin asymmetry is much less affected by variations of  $m$ .

Finally we take a look at the importance of the NLO corrections for the heavy flavor spin asymmetry. Figure 7 shows the ratio of the charm spin asymmetry calculated in NLO (as shown in Fig. 5) and in LO for different sets of helicity densities [18,22,23]. One can infer that the NLO asymmetries are generally *smaller* than the LO ones by a factor of about three. In the case of the AAC helicity densities [22] we find an even larger suppression. The strong dependence on  $x_T^{\text{min}}$  and the choice of parton densities inhibit the use of constant “ $K$  factors” [ $= \tilde{\sigma}(\text{LO})/\tilde{\sigma}(\text{NLO})$ ] to estimate the NLO results from LO ones. It should also be pointed out that much of the reduction of the asymmetry in NLO stems from the *unpolarized* cross section in NLO, which is about a factor of two larger than the corresponding LO result. This is illustrated by the thin solid line in Fig. 7 representing the ratio  $\sigma(\text{LO})/\sigma(\text{NLO})$  obtained with the Glück-Reya-Vogt 1998 (GRV’98) parton densities [26]. The sizable difference of the asymmetry predictions in LO and NLO implies that the LO and NLO gluon helicity densities extracted from a future asymmetry measurement may differ considerably. Whether this will be consistent with data from other processes has to be studied in a “global QCD analysis,” e.g., along the lines suggested in Ref. [27].

Further studies of the uncertainties and predictions for bottom quark production will become available in the near future [10], along with more details concerning the calculational techniques that have been used as well as analytical results for the matrix elements that we have obtained.

#### IV. FURTHER APPLICATIONS AND SUMMARY

Heavy flavor production at RHIC is also interesting for reasons other than  $\Delta g$ . Our results are also required for a fully consistent description of the polarized photoproduction of heavy quark pairs. Apart from the “direct” process  $\gamma g \rightarrow Q\bar{Q}$ , where the NLO corrections have been calculated in Refs. [13,28], the (quasi-)real photon can also resolve into its hadronic content before the hard scattering takes place. The introduction of photonic parton densities is mandatory for a consistent factorization of singularities of the direct process associated with collinear  $\gamma \rightarrow q\bar{q}$ ,  $q = u, d, s$ , splittings. Polarized “resolved” photon processes, Eq. (1), have been estimated [29] to be small for fixed target experiments such as

COMPASS [30], but can be significant at proposed future polarized lepton-hadron colliders such as the BNL Electron Ion Collider (EIC) [31].

In addition, our LO and NLO results for the dominant gluon-gluon fusion subprocess also contain the production of gluino pairs,<sup>3</sup>  $gg \rightarrow \tilde{g}\tilde{g}$ , after adjusting the color factors in Eq. (5) appropriately [4]: replace the prefactor  $1/2(N_C^2 - 1)$  by  $N_C/(N_C^2 - 1)$  and set  $C_F = C_A = N_C$  inside the square brackets. Before doing the latter, one has to use the identity  $1 = C_A^2 - 2C_FC_A$  for the  $KQ$  part, i.e.,  $\tilde{M}_{KQ} = (C_A^2 - 2C_FC_A)\tilde{M}_{KQ} \rightarrow -N_C^2\tilde{M}_{KQ}$ . Supersymmetric scenarios where light gluinos  $\tilde{g}$  exclusively decay into even lighter (s)bottom quarks  $\tilde{b}$  and  $b$ 's,  $\tilde{g} \rightarrow b\tilde{b}$ , have been proposed [32] as a remedy for the longstanding discrepancy between data from the Tevatron collider for unpolarized open  $b$  production and theory [19]. Recently,  $b$  rates in  $ep$  and  $\gamma\gamma$  collisions were also found to be in excess of theoretical predictions [19]. Our results allow estimation of the spin-dependent hadroproduction rates of (light) gluinos at RHIC, as well as at a conceivable polarized version of the CERN Large Hadron Collider (LHC) in the distant future. However, a recent study [33] has revealed that a proper implementation of the  $b$  quark

hadronization can remove a good part of the discrepancy between the Tevatron data and corresponding QCD calculations. Whether this effect can also account for the observed excess in  $ep$  and  $\gamma\gamma$  collisions remains to be checked.

To summarize, we have presented the first complete NLO QCD calculation for the spin-dependent hadroproduction of heavy quarks. The NLO results have considerably fewer uncertainties stemming from variations of the unphysical factorization and renormalization scales and become fairly independent of the scales for the conventional choice  $\mu_F = \mu_R$ . We have presented predictions for the charm asymmetry that can soon be measured at RHIC. These results include an “efficiency” which models the hadronization and decays of the produced heavy quarks, experimental cuts, and detector geometry. As in the unpolarized case, LO calculations cannot be substituted in any simple manner for the full NLO result. As expected, charm production at RHIC turns out to be a useful tool to determine the  $x$  shape of the polarized gluon density  $\Delta g$ .

### ACKNOWLEDGMENTS

We are grateful to M. Grosse Perdekamp and J. Smith for helpful discussions. M.S. thanks SUNY Stony Brook, RIKEN, and Brookhaven National Laboratory for hospitality and support during the final steps of this work. I.B.'s work has been supported by the “Bundesministerium für Bildung, Wissenschaft, Forschung und Technologie” and the Austrian Research Council.

<sup>3</sup>The  $q\bar{q} \rightarrow \tilde{g}\tilde{g}$  subprocess receives new contributions absent in  $q\bar{q} \rightarrow Q\bar{Q}$ .

- [1] European Muon Collaboration (EMC), J. Ashman *et al.*, Phys. Lett. B **206**, 364 (1988); Nucl. Phys. **B328**, 1 (1989); for a recent review of the data on polarized deep-inelastic scattering, see, e.g., E. Hughes and R. Voss, Annu. Rev. Nucl. Part. Sci. **49**, 303 (1999).
- [2] For a recent review of the RHIC spin physics program, see: G. Bunce, N. Saito, J. Soffer, and W. Vogelsang, Annu. Rev. Nucl. Part. Sci. **50**, 525 (2000).
- [3] S.B. Libby and G. Sterman, Phys. Rev. D **18**, 3252 (1978); R.K. Ellis *et al.*, Phys. Lett. **78B**, 281 (1978); Nucl. Phys. **B152**, 285 (1979); D. Amati, R. Petronzio, and G. Veneziano, *ibid.* **B140**, 54 (1980); **B146**, 29 (1978); G. Curci, W. Furmanski, and R. Petronzio, *ibid.* **B175**, 27 (1980); J.C. Collins, D.E. Soper, and G. Sterman, Phys. Lett. **134B**, 263 (1984); Nucl. Phys. **B261**, 104 (1985); J.C. Collins, *ibid.* **B394**, 169 (1993).
- [4] W. Beenakker, H. Kuijf, J. Smith, and W.L. van Neerven, Phys. Rev. D **40**, 54 (1989).
- [5] W. Beenakker, R. Meng, G.A. Schuler, J. Smith, and W.L. van Neerven, Nucl. Phys. **B351**, 507 (1991).
- [6] S. Dawson, R.K. Ellis, and P. Nason, Nucl. Phys. **B327**, 49 (1988).
- [7] S. Dawson, R.K. Ellis, and P. Nason, Nucl. Phys. **B303**, 607 (1988).
- [8] A.P. Contogouris, S. Papadopoulos, and B. Kamal, Phys. Lett. B **246**, 523 (1990).
- [9] M. Karliner and R.W. Robinett, Phys. Lett. B **324**, 209 (1994).
- [10] I. Bojak and M. Stratmann (in preparation).
- [11] N.S. Craigie, K. Hidaka, M. Jacob, and F.M. Renard, Phys. Rep. **99**, 69 (1983).
- [12] G. 't Hooft and M. Veltman, Nucl. Phys. **B44**, 189 (1972); P. Breitenlohner and D. Maison, Commun. Math. Phys. **52**, 11 (1977).
- [13] I. Bojak and M. Stratmann, Phys. Lett. B **433**, 411 (1998); Nucl. Phys. **B540**, 345 (1999); **B569**, 694(E) (2000).
- [14] G. Passarino and M. Veltman, Nucl. Phys. **B160**, 151 (1979); W. Beenakker, Ph.D. thesis, University of Leiden, 1989.
- [15] I. Bojak, Ph.D. thesis, University of Dortmund, 2000, hep-ph/0005120.
- [16] N. Kidonakis, E. Laenen, S. Moch, and R. Vogt, Phys. Rev. D **64**, 114001 (2001).
- [17] W. Vogelsang, Phys. Rev. D **54**, 2023 (1996); Nucl. Phys. **B475**, 47 (1996).
- [18] M. Glück, E. Reya, M. Stratmann, and W. Vogelsang, Phys. Rev. D **63**, 094005 (2001).
- [19] Recent results on  $b$  production can be found, e.g., in F. Sefkow, J. Phys. G **28**, 953 (2002).
- [20] T. Sjöstrand, L. Lönnblad, and S. Mrenna, hep-ph/0108264.
- [21] E. Norrbin and T. Sjöstrand, Eur. Phys. J. C **17**, 137 (2000).
- [22] Asymmetry Analysis Collaboration, Y. Goto *et al.*, Phys. Rev. D **62**, 034017 (2000).
- [23] D. de Florian and R. Sassot, Phys. Rev. D **62**, 094025 (2000).
- [24] M. Glück, E. Reya, M. Stratmann, and W. Vogelsang, Phys. Rev. D **53**, 4775 (1996).
- [25] T. Gehrmann and W.J. Stirling, Phys. Rev. D **53**, 6100 (1996).



- [26] M. Glück, E. Reya, and A. Vogt, *Eur. Phys. J. C* **5**, 461 (1998).
- [27] M. Stratmann and W. Vogelsang, *Phys. Rev. D* **64**, 114007 (2001).
- [28] A.P. Contogouris, G. Grispos, and Z. Merebashvili, *Phys. Lett. B* **482**, 93 (2000); Z. Merebashvili, A.P. Contogouris, and G. Grispos, *Phys. Rev. D* **62**, 114509 (2000).
- [29] M. Stratmann and W. Vogelsang, *Z. Phys. C* **74**, 641 (1997).
- [30] COMPASS Collaboration, G. Baum *et al.*, Report No. CERN/SPSLC 96-14; Report No. CERN/SPSLC 96-30.
- [31] See <http://www.bnl.gov/eic> for information concerning the EIC project, including the EIC whitepaper.
- [32] E.L. Berger *et al.*, *Phys. Rev. Lett.* **86**, 4231 (2001); E.L. Berger, in *Heavy Flavor Physics*, Proceedings of the Ninth International Symposium on Heavy Flavor Physics, Pasadena, California, 2001, edited by A. Ryd and F.C. Porter, AIP Conf. Proc. No. 618 (AIP, Melville, NY, 2002), p. 317.
- [33] M. Cacciari and P. Nason, *Phys. Rev. Lett.* **89**, 122003 (2002).